Emerging ground and excited state dipole moments and external electric field effect on electronic structure. A solvatochromism and theoretical study on 2-((phenylimino)methyl)pheno...

ARTICLE · JANUARY 2015

DOI: 10.1016/2015.01.056

4 AUTHORS, INCLUDING:

Isa Sidir
Bitlis Eren University
20 PUBLICATIONS **141** CITATIONS
SEE PROFILE

Halil Berber
Anadolu University
38 PUBLICATIONS **117** CITATIONS
SEE PROFILE

Journal of Molecular Liquids 206 (2015) 56–67

Contents lists available at ScienceDirect

Journal of Molecular Liquids

journal homepage: www.elsevier.com/locate/molliq

Emerging ground and excited state dipole moments and external electric field effect on electronic structure. A solvatochromism and theoretical study on 2-((phenylimino)methyl)phenol derivatives

İsa Sıdır [a,*], Yadigar Gülseven Sıdır [a], Halil Berber [b], Ferhat Demiray [c]

[a] Bitlis Eren University, Faculty of Arts & Science, Department of Physics, 13000 Bitlis, Turkey
[b] Anadolu University, Faculty of Science, Department of Chemistry, 26470 Eskişehir, Turkey
[c] Abant İzzet Baysal University, Vocational Higher School, Mudurnu, Bolu, Turkey

ARTICLE INFO

Article history:
Received 4 November 2014
Received in revised form 7 January 2015
Accepted 30 January 2015
Available online 2 February 2015

Keywords:
Schiff base
Dipole moment
Solvatochromic shift
Electric field
Density of state
LSER
DFT
LDA
GGA

ABSTRACT

The absorption and fluorescence spectra of three 2-((phenylimino)methyl)phenol derivatives have been evaluated in a series of organic solvents. The ground state (μ_g) and excited state (μ_e) dipole moments are determined by means of Lippert–Mataga, Bakhshiev, Kaski–Chamma–Viallet and Reichardt solvatochromic shift methods based on the solvent polarity parameters. Excited state dipole moments are found as larger than the ground state dipole moment due to substantial redistribution of the π-electron density in more polar excited state and thus resonance structures of 2-((phenylimino)methyl)phenol derivatives are analyzed. Solute–solvent interactions are analyzed by means of linear solvation energy relationships (LSER) using dielectric constant function $f(\varepsilon)$, refractive index function $f(n)$ and Kamlet–Taft parameters (H-bond donor ability, α and H-bond acceptor ability, β). External electric field (EF) effect on HOMO–LUMO gap (HLG) and dipole moment are investigated by B3LYP, LDA and GGA methods. Density of states (DOS) and HOMO, LUMO plots are also investigated by the same methods.

1. Introduction

Schiff bases have wide applications in medicine, pharmaceutical, industrial, chemosensor chemistry and biological processes [1–7]. Proton tautomerism plays a significant role in various fields of chemistry and biochemistry [8]. 2-Hydroxy Schiff bases exhibit enol and keto tautomeric arrangements between OH and NH forms giving rise to differences in electronic absorption and fluorescence spectra [9–12]. Schiff bases which have solvent dependent UV–vis spectra can be considered as NLO (nonlinear optical) materials [13]. Variable temperature X-ray crystallographic analyses of 2-hydroxy Schiff base indicate that enol form is usually more stable than the keto form [14]. The keto form is predominantly zwitterionic in crystals and stabilized in crystals by hydrogen bonding and electrostatic intermolecular interactions [15–20]. Most of these studies were focused on the determination of tautomeric preferences, and investigation of the role of substituents on the position of the tautomeric equilibria, solvato-, iono-, thermo- and photochromic effects [21–31]. Photochromic compounds are important because of their use as optical switches and optical memories, variable electrical current, ion transport through membrane. In addition, they have widespread usage as ligands in the field of coordination chemistry as well as in diverse fields of chemistry and biochemistry owing to their biological activities [32–34]. Thermochromism and photochromism in Schiff base are related to tautomerism, molecular geometry (planar and non-planar, respectively) and crystal packing of the crystal [32,35,36]. Tautomeric Schiff bases can serve as the specific type of molecular switches in optical recording technology, molecular electronics and computing [37,38]. The last research indicates that monomer and polymer Schiff bases are promising materials for using as electron donor in photovoltaic organic cells due to their designable HOMO–LUMO gap energies [39].

In the present work, we have determined the ground state and excited state dipole moments of ip1, ip2 and ip3 by means of Lippert–Mataga, Bakhshiev, Kaski–Chamma–Viallet and Reichardt solvatochromic shift methods. Solvent effects on absorption and fluorescence spectra are evaluated. A detailed theoretical investigation has been performed on external electric field (EF) effect on

* Corresponding author.
E-mail addresses: isidir@beu.edu.tr, isa.sidir@gmail.com (İ. Sıdır).

http://dx.doi.org/10.1016/j.molliq.2015.01.056
0167-7322/

dipole moment and HOMO–LUMO gap (HLG). Density of states (DOS) and HOMO, LUMO plots are investigated by generalized gradient approximation (GGA) method.

2. Materials and methods

2.1. Theoretical background

The electric dipole moment of a polar solute polarizes the solvent so that the solute itself experiences an electric field, the reaction field, which is proportional to the solute dipole moment in the ground and excited states. Such proportionalities for the difference and sum of absorption, $\tilde{\nu}_a$, and fluorescence, $\tilde{\nu}_f$, maxima (in cm^{-1}) have been defined by following equations:

$$\tilde{\nu}_a - \tilde{\nu}_f = m_{L-M} F_{Lippert-Mataga}(\varepsilon, n) + \text{constant} \quad (1)$$

$$\tilde{\nu}_a - \tilde{\nu}_f = m_B F_{Bakhshiev}(\varepsilon, n) + \text{constant} \quad (2)$$

$$\left(\tilde{\nu}_a + \tilde{\nu}_f\right)/2 = -m_{K-C-V} F_{Kawski-Chamma-Viallet}(\varepsilon, n) + \text{constant} \quad (3)$$

where

$$m_{L-M} = 2\left(\mu_e - \mu_g\right)^2 / hca_0^3 \quad (4)$$

$$m_B = 2\left(\mu_e - \mu_g\right)^2 / hca_0^3 \quad (5)$$

$$m_{K-C-V} = 2\left(\mu_e^2 - \mu_g^2\right)/hca_0^3. \quad (6)$$

The symbols h and c are Planck's constant and the velocity of light in vacuum, respectively. $F_{Lippert-Mataga}$ [40], $F_{Bakhshiev}$ [41], and $F_{Kawski-Chamma-Viallet}$ [42,43] are solvent polarity functions and are given as:

$$F_{Lippert-Mataga}(\varepsilon, n) = \frac{\varepsilon - 1}{2\varepsilon + 1} - \frac{n^2 - 1}{2n^2 + 1} \quad (7)$$

$$F_{Bakhshiev}(\varepsilon, n) = \frac{2n^2 + 1}{n^2 + 2}\left[\frac{\varepsilon - 1}{\varepsilon + 2} - \frac{n^2 - 1}{n^2 + 2}\right] \quad (8)$$

$$F_{Kawski-Chamma-Viallet}(\varepsilon, n) = \left[\frac{2n^2 + 1}{2(n^2 + 2)}\left(\frac{\varepsilon - 1}{\varepsilon + 2} - \frac{n^2 - 1}{n^2 + 2}\right) + \frac{3\left(n^4 - 1\right)}{2(n^2 + 2)^2}\right]. \quad (9)$$

The other symbols ε and n are dielectric constant and refractive index of the solvents, respectively. Employing linear curve fitting route for $\tilde{\nu}_a - \tilde{\nu}_f$ versus $F_{Lippert-Mataga}$, $\tilde{\nu}_a - \tilde{\nu}_f$ versus $F_{Bakhshiev}$ and $(\tilde{\nu}_a + \tilde{\nu}_f)/2$ versus $F_{Kawski-Chamma-Viallet}$ gives m_{L-P}, m_B and m_{K-C-V}, respectively. If it can be supposed that ground- and excited-state dipole moments are parallel, then:

$$\mu_g = \frac{m_{K-C-V} - m_B}{2}\left(\frac{hca^3}{2m_B}\right)^{1/2}, \quad (10)$$

$$\mu_e = \frac{m_{K-C-V} + m_B}{2}\left(\frac{hca^3}{2m_B}\right)^{1/2}, \quad (11)$$

$$\mu_e = \frac{m_{K-C-V} + m_B}{m_{K-C-V} - m_B}\mu_g, (m_{K-C-V} \rangle m_B). \quad (12)$$

Moreover, the Reichardt method based on the empirical polarity scale, E_T^N [44], can be used for estimating dipole variation ($\Delta\mu$) from solvatochromic shift. The theoretical basis for the correlation of the spectral shift with E_T^N has been developed by Ravi et al. [45]:

$$\tilde{\nu}_a - \tilde{\nu}_f = 11307.6\left[\left(\frac{\Delta\mu}{\Delta\mu_B}\right)^2\left(\frac{a_B{}^B}{a_0}\right)^3\right]E_T^N + \text{constant} \quad (13)$$

where $\Delta\mu_B = 9D$ and $a_B = 6.2$ Å are the change in dipole moment on excitation and Onsager radius of reference betaine dye, respectively. $\Delta\mu$ and a_0 are the corresponding dipole moment change and Onsager radius for the solute molecule. The change in dipole moment $\Delta\mu$, can be determined as:

$$\mu_e - \mu_g = \sqrt{\frac{m_{E_T^N} x 81}{11307.6 x (6.2/a_0)^3}} \quad (14)$$

where $m_{E_T^N}$ is the slope obtained from the linear plot of Stokes shift as indicated in Eq. (15).

$$\overline{\nu}_a - \overline{\nu}_f = m_{E_T^N} E_T^N + \text{constant} \quad (15)$$

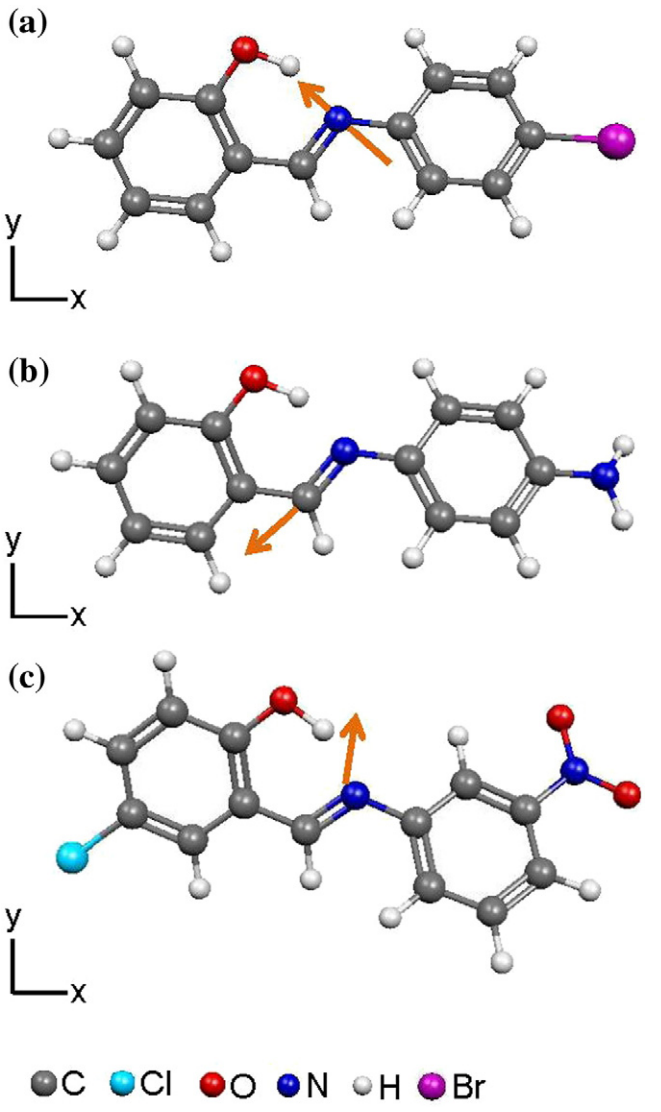

Fig. 1. GGA optimized molecular structures and direction of ground state dipole moment of (a) ip1, (b) ip2 and (c) ip3 molecules.

2.2. Experimental details

ip1, ip2 and ip3 (Fig. 1) were synthesized by the method given in the reference [46]. All of the solvents were of spectroscopic grade commercially available from Sigma-Aldrich. All of the solvents were checked in steady-state fluorescence apparatuses for the lack of fluorescence impurities in the wavelength ranges of interest. The concentrations of the solutions were prepared as 3.4×10^{-5} M. Ultraviolet–visible (UV–vis) absorption spectra were recorded on a Perkin Elmer Lambda-35 UV–vis Spectrophotometer over a wavelength range of 200–800 nm. Steady-state fluorescence spectra were recorded on Perkin Elmer LS-55 Fluorescence Spectrometer by choosing excitation wavelength 362 nm for ip1, 437 nm for ip2 and 399 nm for ip3. ip1, ip2 and ip3 molecules do not show excitation wavelength dependence. In order to record the fluorescence spectra, excitation wavelengths are chosen as that fluorescence spectrum is obtained at the highest intensity and at the highest resolution. Therefore, we have chosen these excitation wavelengths. The excitation source was a long life xenon flash lamp. All of the measurements were performed using 1 cm × 1 cm quartz cell at room temperature. The positions of the absorption and fluorescence bands were determined by Gaussian curve fit analysis using OriginPro 7.5. Linear correlation and data fit were also performed by using OriginPro 7.5. Dielectric constant, ε, refractive index, n were taken from the literature [47–50].

2.3. Computational method

We used density functional theory (DFT) implemented with B3LYP/6-311 + G(d) level of theory [51] for optimization and frequency calculation which confirms that there is no imaginary frequency in the optimized geometry indicating true energy minima. All calculations were carried out in Gaussian 09W program [52].

External EF effect on HLG and μ_g was investigated by using B3LYP, LDA and GGA method. DOS and HOMO, LUMO plots were also calculated by the same methods. Geometry optimization and total energy calculations were based on the spin polarized DFT in the Local Density Approximation (LDA) and Generalized Gradient Approximation (GGA) as implemented in the SIESTA code [53]. We used Perdew–Burke–Ernzerhof [54] GGA functional and Perdew–Zunger parametrization for the LDA functional [55]. Electronic wavefunctions were expanded to a double-ζ basis set augmented by polarization orbitals. The interactions between the core and valance electrons were handled by Troullier–Martins norm-conserving pseudopotentials [56] in their fully separable form [57]. The geometry optimizations in the conjugate-gradient algorithm were continued until all force components are less than 0.01 eV/Å.

2.4. Onsager cavity radius

The value of Onsager cavity radiuses (a_0) of ip1, ip2 and ip3 are calculated from the following equation [58],

$$a_0 = \left(\frac{3M}{4\pi d N_A}\right)^{1/3} \tag{16}$$

where d is the density of solute molecule, M the molecular weight of the solute molecule and N_A is the Avagadro's number. Densities and molecular weights are $d = 1.547$ (g/cm^3) and $M = 276.13$ (g/mol) for ip1, $d = 1.298$ (g/cm^3) and $M = 212.25$ (g/mol) for ip2, $d = 1.439$ (g/cm^3) and $M = 276.68$ (g/mol) for ip3, respectively. Thus, a_0 is found to be 4.221 Å, 4.099 Å and 4.327 Å for ip1, ip2 and ip3, respectively. Densities were calculated with $d = \frac{M}{V}$ equation based on molar volume (V) computed using DFT-B3LYP/6-311++G(d,p) method.

2.5. Multiple linear regression analysis details

Linear solvation energy relationships (LSER) have been used to determine solute and solvent interactions of investigated compounds. LSER determine to the specific/nonspecific interactions and intra/inter molecular interactions in electronic transition mechanisms of solute molecules in solvent medium. The LSER approach is preferable because it has been successfully applied to the positions or intensities of maximal absorption in UV–visible absorption and fluorescence spectra [59]. The LSERs (linear solvation energy relationships) is determined with below equation,

$$\nu_{max} = C_0 + C_1 \cdot f(n) + C_2 \cdot f(\varepsilon) + C_3 \cdot \beta + C_4 \cdot \alpha \tag{17}$$

where: ν_{max} are defined to maximum absorption band depending on solvent of molecules; $f(\varepsilon)$ and $f(n)$ are characterized as dielectric function ($f(\varepsilon) = (\varepsilon - 1) / (\varepsilon + 2)$) and refractive index function ($f(n) = (n^2 - 1) / (n^2 + 1)$), respectively. The β and α (Kamlet–Taft parameters) are determined as hydrogen bonding acceptor ability and hydrogen bonding donor ability, respectively. The C_0 coefficient has determined maximum absorption band in gaseous phase. The C_1 coefficient value is representing orientation induction interaction according to the frequency shift, while C_2 coefficient represents the dispersion polarization interactions to it. The C_3 and C_4 coefficient values have shown contributions done to electronic transitions of hydrogen bond donor ability and hydrogen bond acceptor ability. The MLRA (multiple linear regression analysis) is performed using SPSS 15.0 program.

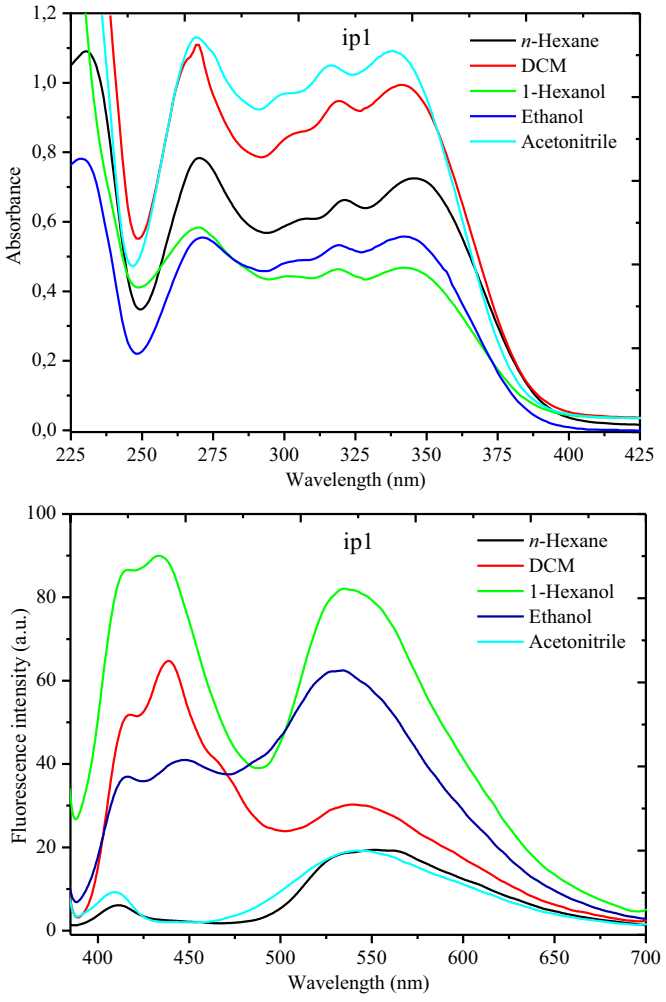

Fig. 2. Absorption and fluorescence spectra of ip1 in selected solvents.

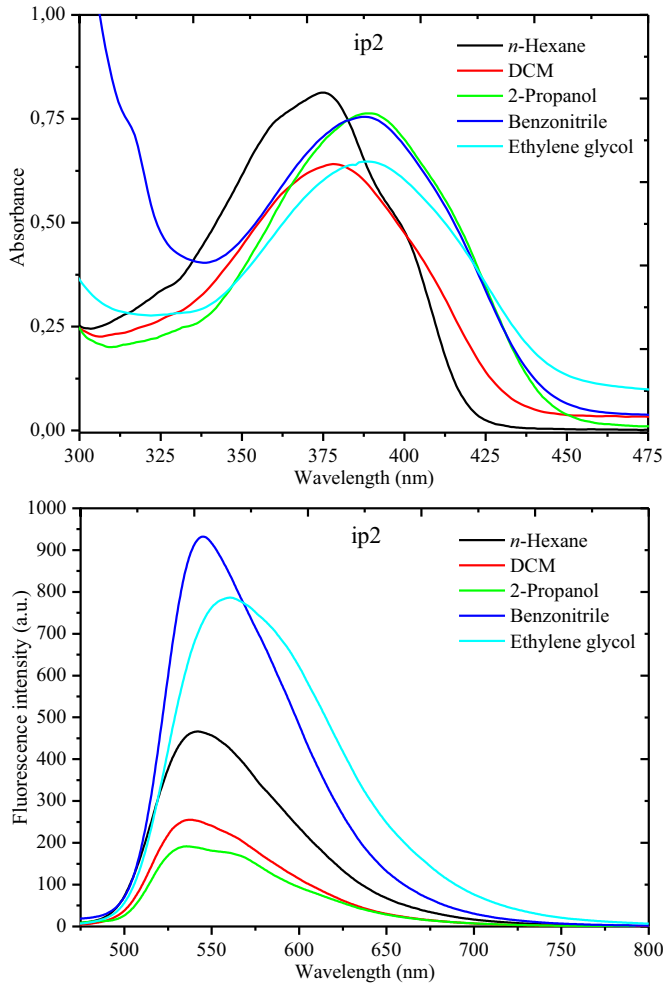

Fig. 3. Absorption and fluorescence spectra of ip2 in selected solvents.

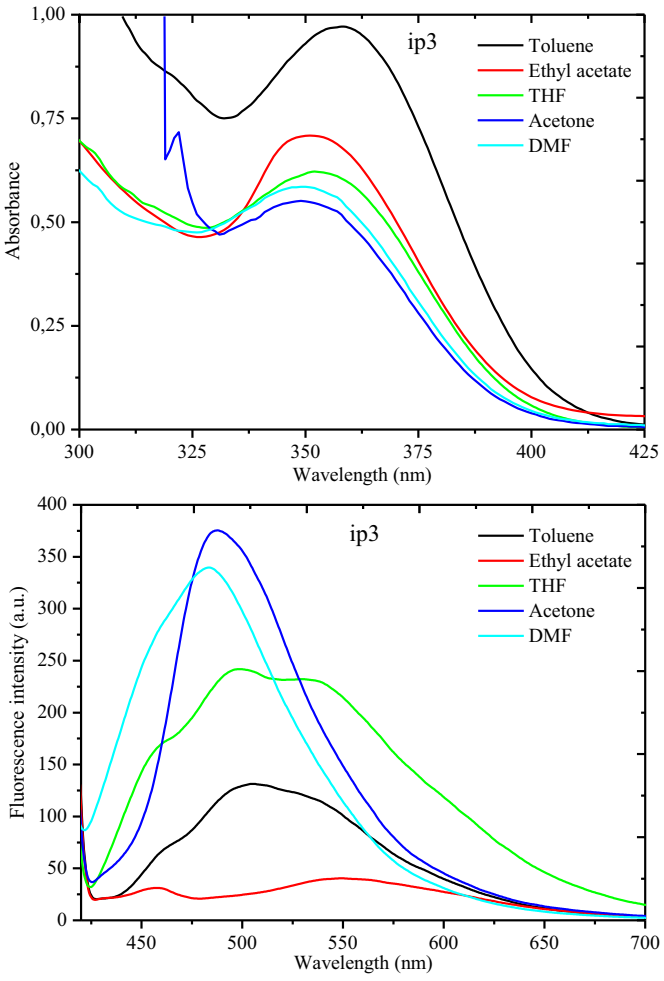

Fig. 4. Absorption and fluorescence spectra of ip3 in selected solvents.

3. Results and discussions

3.1. Solvent effects on the absorption and fluorescence spectra

Steady state absorption and fluorescence spectra of ip1, ip2 and ip3 in different solvents are given in Figs. 2–4. Absorption, emission maximum wavelengths and wavenumbers along with Stokes shift values are listed in Tables 1–2, respectively. Stokes shift does not change regularly with the change of solvent polarity for ip2. However, Stokes shifts of ip1 and ip3 tend to be decreasing with the very low correlation coefficients while increasing of solvent polarity which indicates that molecular geometry change is restricted under excitation (see Supplementary material Fig. S1).

The largest Stokes shifts are observed in *n*-butyl acetate for ip1, *n*-hexane for ip2 and ethylene glycol for ip3 as 11,144, 8216 and 10,723 cm^{-1} respectively (see Table 2). Fluorescence and UV–vis spectra of the studied compounds display one band along with shoulder band in some solvents. Absorption band maxima are observed in the range of 339–346 nm, 374–392 nm and 345–358 nm for ip1, ip2 and ip3, respectively. Fluorescence bands are recorded at the spectrum region of 451–552 nm for ip1, 533–560 nm for ip2 and 483–568 nm for ip3. They are assigned to π–π* electronic transitions due to delocalization in aromatic rings and conjugation between –C═N–N bridge. Second peaks observed in absorption and fluorescence spectra are attributed to n–π* which comes from the lope-pair and solvent interaction. Considering all of the solvent in general trend, it is observed from the absorption spectra that ip1 and ip3 undergo hypsochromic shift with increase of solvent polarity, whereas absorption bands of ip2 tend to bathochromic shift with the solvent polarity change. Emission bands of ip1 and ip3 tend to hypsochromic shift with the increase of solvent polarity, whereas ip2 suffer bathochromic shift while increasing solvent polarity (see Supplementary material Fig. S2). As seen from Table 1, it can be said that fluorescence spectra is relatively more sensitive to solvent induce, solute–solvent interactions and conformational change compared to that of absorption spectra.

Interaction of lone pairs of OH substituent with the solvent and formation of intermolecular and intramolecular O–H—N hydrogen bonding between hydroxyl group and nitrogen atom gives rise to formation of charge transfer. OH group has a mesomerically electron repulsive character and gives rise to system to get rich with electrons. Maximum absorption wavelength of (*E*)-2-((phenylimino)methyl)phenol in methanol is measured as 341 nm [60]. In ip1 molecule, Br has an inductive electron withdrawing character ($\sigma_{p\text{-}Br} = 0.23$) [61] and it is expected that λ_{max} in absorption spectra of ip1 shifts to blue region. However, halogens are mesomerically electron repulsive to the system linked to it and thus increase the electron density of the system [62]. This case leads the absorption λ_{max} to shift to the red region. In ip2 molecule, NH_2 has electron repulsive character ($\sigma_{p\text{-}NH_2} = -0.66$) [61] and gives rise to absorption λ_{max} exposures bathochromic shift. Halogen effect observed in ip1 molecule is applicable for ip3. Cl atom has also an electron withdrawing character ($\sigma_{m\text{-}Cl} = 0.37$) [61]. NO_2 substituent is strong electron withdrawing moiety ($\sigma_{m\text{-}NO_2} = 0.71$) [61] and as expected absorption λ_{max} shifts to lower wavelength. In ip3 molecule, Cl and NO_2 substituents are located at *meta* position of phenyl rings. Substituents located at *meta* position forces to resonance to be effective on the rings not overall the molecule

Table 1
Absorption and fluorescence spectral data for ip1, ip2 and ip3.

No	Solvent	ip1		ip2		ip3	
		λ_{abs} (nm)	λ_{PL} (nm)	λ_{abs} (nm)	λ_{PL} (nm)	λ_{abs} (nm)	λ_{PL} (nm)
1	*n*-Pentane	343	542	374;395(sh)	533; 555(sh)	356	555
2	*n*-Hexane	345	552	375;396(sh)	542	358	554;573
3	Cyclohexane	344	549	376;398(sh)	542	357	563
4	1,4-Dioxane	346	545	382	542	353	545
5	Benzene	344	548	381	537; 557(sh)	354	–
6	Toluene	346	551	382	542	357	505; 525(sh)
7	o-Xylene	345	545	381	537;556(sh)	353	549
8	Diethylether	342	539	380	534;551(sh)	352	542
9	Chloroform	344	547	379	535; 548(sh)	356	557;576
10	Ethyl acetate	344	548	381	541	351	549
11	*n*-Butyl acetate	341	550	382	535;549(sh)	348	552
12	THF	343	–	386	541	353	499;531
13	DCM	341	539	378	538	351	–
14	1-Octanol	343	543	393	538	–	–
15	1-Heptanol	343	543	392	539	352	547;585
16	1-Hexanol	343	537	391	538	350	544
17	1-Butanol	342	520	390	542	350	500
18	iso-Butanol	340	543	389	540	–	–
19	2-Propanol	342	514	389	535;554(sh)	352	552
20	Acetone	341	547	381	542	349	488
21	1-Propanol	341	540	389	544	350	546
22	Ethanol	342	531	385	542	351	501
23	Benzonitrile	342	547	387	545	–	–
24	Methanol	341	451	383	542	350	493
25	DMF	343	479	389	536;553(sh)	349	483
26	Acetonitrile	339	542	378	541	345	–
27	Ethylene glycol	340	545	388	560	353	568
28	DMSO	343	485	392	542	349	487

(see black and purple lines in Fig. 5(c)). This causes the OH group to be dominantly effective on moiety in n–π* and π–π* electronic transitions.

3.2. Estimation of ground and excited state dipole moments

In order to determine the ground state and excited state dipole moments of ip1, ip2 and ip3, we firstly apply Eqs. (1)–(3) and (15) based on the solvatochromic shift methods. Slopes (m), intercepts and correlation coefficients obtained from the plot of $\widetilde{\nu}_a - \widetilde{\nu}_f$ and $(\widetilde{\nu}_a + \widetilde{\nu}_f)/2$ versus solvent polarity function $F(\varepsilon, n)$ and solvent polarity parameter E_T^N by using Lippert–Mataga, Bakhshiev, Kawski–Chamma–Viallet and Reichardt equations are given in Tables 3 and 4. $\widetilde{\nu}_a - \widetilde{\nu}_f$ and $(\widetilde{\nu}_a + \widetilde{\nu}_f)/2$ values and solvent functions and parameters are also given in Tables 2 and 3, respectively. As can be seen from Table 4, correlation coefficients are larger than 0.9078 in most cases which indicate a good linearity for these correlations.

Dipole moments of the ground state (μ_g) are determined from the slopes m_{K-C-C} and m_B of the Kawski–Chamma–Viallet and Bakhshiev correlations by applying Eq. (10). The excited state dipole moments (μ_e) are also determined from slopes (m_{L-M}, m_B, m_{K-C-V} and $m_{E_T^N}$) of Lippert–Mataga, Bakhshiev, Kawski–Chamma–Viallet and Reichardt correlations by applying Eqs. (4)–(6) and (14). All of the results are presented in Table 5.

As presented in Table 5, the ground state dipole moment (Δ_g) of ip1 (4.236 D) is found as larger than those of ip2 (1.782 D) and ip3 (3.709 D) due to the resonance structures of the compounds. In the ip1 molecule, OH substituent ($\sigma_{p\text{-}OH} = -0.37$) has electron pushing character whereas Br is electron withdrawing atom as inductive. As seen from Fig. 5(a), possible resonance is towards the phenyl ring in which Br atom linked to it and thus charge irregularity occurs composing a dipole. In the ip2 molecule, both OH ($\sigma_{p\text{-}OH} = -0.37$) and NH_2 ($\sigma_{p-NH_2} = -0.66$) substituents have electron pushing character with different intensity. Possible resonance structure given in Fig. 5(b) indicates relatively lower charge irregularity and consequently smaller dipole moment for ip2. ip3 molecule

Table 2
Experimental absorption and fluorescence wavelengths for ip1, ip2 and ip3.

No	Solvents	ip1					ip2					ip3				
		$\overline{\nu}_a$	$\overline{\nu}_f$	$\overline{\nu}_a - \overline{\nu}_f$	$\overline{\nu}_a + \overline{\nu}_f$	$(\overline{\nu}_a + \overline{\nu}_f)/2$	$\overline{\nu}_a$	$\overline{\nu}_f$	$\overline{\nu}_a - \overline{\nu}_f$	$\overline{\nu}_a + \overline{\nu}_f$	$(\overline{\nu}_a + \overline{\nu}_f)/2$	$\overline{\nu}_a$	$\overline{\nu}_f$	$\overline{\nu}_a - \overline{\nu}_f$	$\overline{\nu}_a + \overline{\nu}_f$	$(\overline{\nu}_a + \overline{\nu}_f)/2$
1	*n*-Pentane	29,155	18,450	10,704	47,605	23,802	26,738	18,762	7976	45,500	22,750	28,090	18,018	10,072	46,108	23,054
2	*n*-Hexane	28,986	18,116	10,870	47,101	23,551	26,667	18,450	8216	45,117	22,558	27,933	18,051	9882	45,984	22,992
3	Cyclohexane	29,070	18,215	10,855	47,285	23,642	26,596	18,450	8146	45,046	22,523	28,011	17,762	10,249	45,773	22,887
4	1,4-Dioxane	28,902	18,349	10,553	47,250	23,625	26,178	18,450	7728	44,628	22,314	28,329	18,349	9980	46,677	23,339
5	Benzene	29,070	18,248	10,822	47,318	23,659	26,247	18,622	7625	44,869	22,434	28,248	–	–	–	–
6	Toluene	28,902	18,149	10,753	47,051	23,525	26,178	18,450	7728	44,628	22,314	28,011	19,802	8209	47,813	23,907
7	o-Xylene	28,986	18,349	10,637	47,334	23,667	26,247	18,622	7625	44,869	22,434	28,329	18,215	10,114	46,544	23,272
8	Diethylether	29,240	18,553	10,687	47,793	23,896	26,316	18,727	7589	45,042	22,521	28,409	18,450	9959	46,859	23,430
9	Chloroform	29,070	18,282	10,788	47,351	23,676	26,385	18,692	7694	45,077	22,538	28,090	17,953	10,137	46,043	23,022
10	Ethyl acetate	29,070	18,248	10,822	47,318	23,659	26,247	18,484	7762	44,731	22,366	28,490	18,215	10,275	46,705	23,352
11	*n*-Butyl acetate	29,326	18,182	11,144	47,507	23,754	26,178	18,692	7486	44,870	22,435	28,736	18,116	10,620	46,852	23,426
12	THF	29,154	–	–	–	–	25,907	18,484	7422	44,391	22,196	28,329	20,040	8289	48,369	24,184
13	DCM	29,326	18,553	10,773	47,878	23,939	26,455	18,587	7868	45,042	22,521	28,490	–	–	–	–
14	1-Octanol	29,155	18,416	10,738	47,571	23,785	25,445	18,587	6858	44,033	22,016	–	–	–	–	–
15	1-Heptanol	29,155	18,416	10,738	47,571	23,785	25,510	18,553	6957	44,063	22,032	28,409	18,282	10,128	46,691	23,345
16	1-Hexanol	29,155	18,622	10,533	47,776	23,888	25,575	18,587	6988	44,163	22,081	28,571	18,382	10,189	46,954	23,477
17	1-Butanol	29,240	19,231	10,009	48,471	24,235	25,641	18,450	7191	44,091	22,046	28,571	20,000	8571	48,571	24,286
18	iso-Butanol	29,412	18,416	10,996	47,828	23,914	25,707	18,519	7188	44,225	22,113	–	–	–	–	–
19	2-Propanol	29,240	19,455	9785	48,695	24,348	25,707	18,692	7015	44,399	22,199	28,409	18,116	10,293	46,525	23,263
20	Acetone	29,326	18,282	11,044	47,607	23,804	26,247	18,450	7797	44,697	22,348	28,653	20,492	8161	49,145	24,573
21	1-Propanol	29,326	18,519	10,807	47,844	23,922	25,707	18,382	7325	44,089	22,045	28,571	18,315	10,256	46,886	23,443
22	Ethanol	29,240	18,832	10,407	48,072	24,036	25,974	18,450	7524	44,424	22,212	28,490	19,960	8530	48,450	24,225
23	Benzonitrile	29,240	18,282	10,958	47,521	23,761	25,840	18,349	7491	44,188	22,094	–	–	–	–	–
24	Methanol	29,326	22,173	7153	51,498	25,749	26,110	18,450	7659	44,560	22,280	28,571	20,284	8287	48,855	24,428
25	DMF	29,155	20,877	8278	50,031	25,016	25,707	18,657	7050	44,364	22,182	28,653	20,704	7949	49,357	24,679
26	Acetonitrile	29,499	18,450	11,048	47,949	23,974	26,455	18,484	7971	44,939	22,470	28,985	–	–	–	–
27	Ethylene glycol	29,412	18,349	11,063	47,760	23,880	25,773	17,857	7916	43,630	21,815	28,329	17,606	10,723	45,934	22,967
28	DMSO	29,155	20,619	8536	49,773	24,887	25,510	18,450	7060	43,960	21,980	28,653	20,534	8119	49,187	24,594

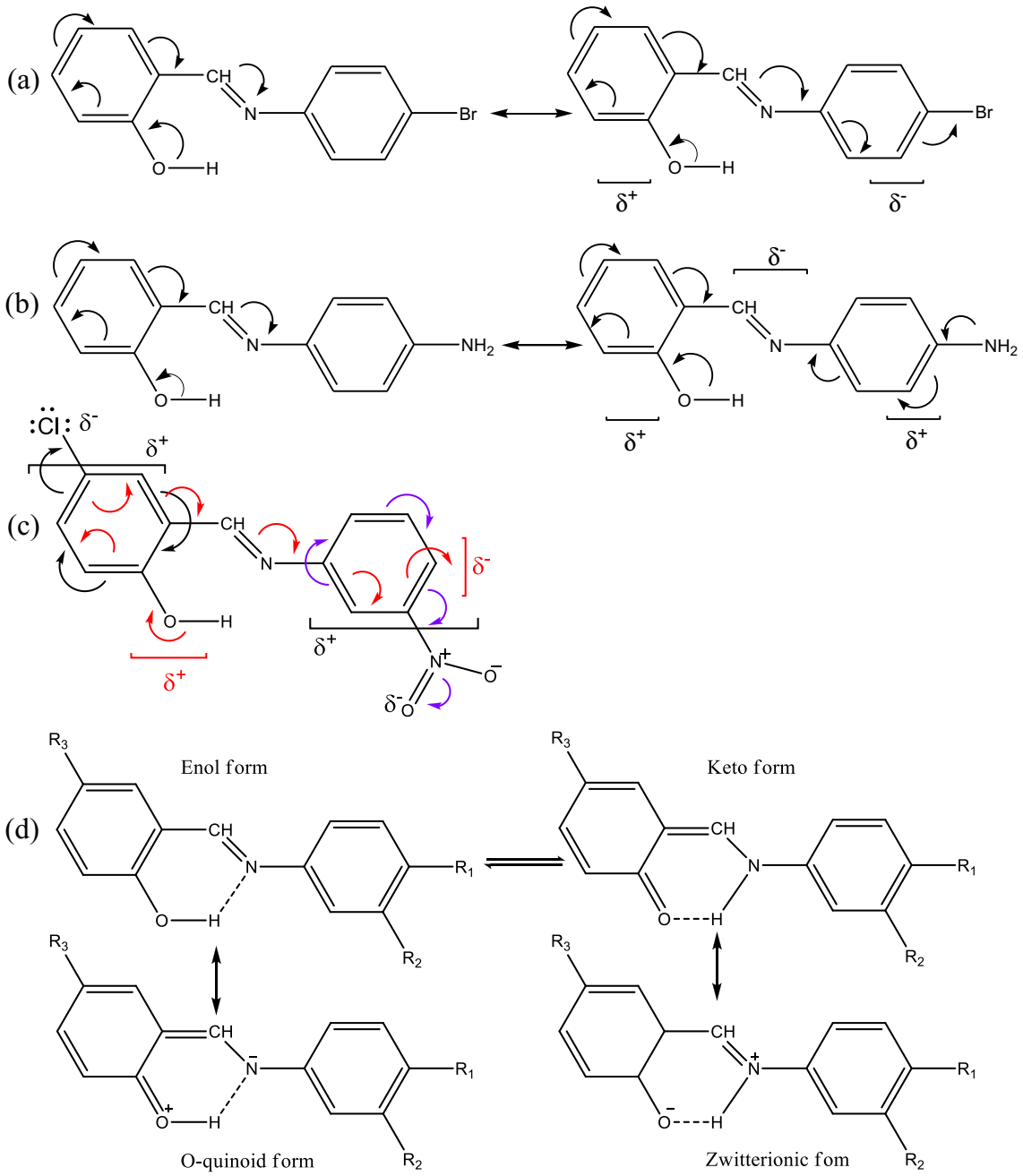

Fig. 5. Possible resonance structures, tautomer and ionic forms of ip1, ip2 and ip3.

has three different substituents as OH, Cl and NO_2. NO_2 moiety is electron withdrawing group whereas OH and Cl have electron pushing character. As can be seen from Fig. 5(c), ip3 molecule has three separate resonance channels. The channel shown by black curved lines indicates the possible resonance formed between phenyl ring and Cl. The channel shown by violet curved lines are demonstration of possible resonance that occurred between phenyl ring and NO_2 group. The red lines specify the possible resonance along the whole compound starting from OH group. These resonance structures give rise to ip3 that has irregular charge distribution resulted in pronounced dipole. In accordance with the resonance structures, it is expected that ground state dipole moments are ordered as $\mu_g(ip1) \rangle \mu_g(ip3) \rangle \mu_g(ip2)$ in consistency with the findings in Table 5.

Excited state dipole moments are obtained higher than ground state dipole moment for all of the studied molecules which indicate that studied Schiff base derivatives are significantly more polar in their excited state than in their ground state. Discrepancies between ground and excited state dipole moments can be explained with the nature of emitting state, substituent effect, charge transfer, resonance structures (Fig. 5(d)) and conformational change occuring under excitation. Resonance structures arise out of delocalization of π-electrons with the interactions by the way of enol-keto tautomerism and formation of ionic structure. It is noticed that μ_e calculated from solvatochromic shift methods show differences, since they use different solvent polarity functions. Theoretically estimated ground state dipole moment directions can be seen in Fig. 1.

3.3. Electric field effect on dipole moment and HOMO–LUMO gap

The variations of HOMO–LUMO gap (HLG) versus the external electric field (EF) in the x, y, z, and xyz-directions are depicted in Fig. 6. As can be

Table 3
Solvent parameters and solvent polarity functions.

No	Solvent	ε	n	β	α	$f(\varepsilon)$	$f(n)$	$f(\varepsilon,n)$	$f(\varepsilon,n)+2g(n)$	$F_{L-M}(\varepsilon,n)$[a]	$F_B(\varepsilon,n)$[b]	$F_{K-C-W}(\varepsilon,n)$[c]	E_T^N [d]
1	*n*-Pentane	1.84	1.3575	0.00	0.00	0.218	0.296	−0.0006	0.4860	−0.0004	−0.0006	0.2430	0.009
2	*n*-Hexane	1.88	1.3749	0.00	0.00	0.226	0.308	−0.0025	0.5076	−0.0014	−0.0025	0.2538	0.009
3	Cyclohexane	2.02	1.4266	0.00	0.00	0.253	0.341	−0.0035	0.5754	−0.0018	−0.0035	0.2877	0.006
4	1,4-Dioxane	2.21	1.4224	0.37	0.00	0.287	0.338	0.0415	0.6148	0.0205	0.0415	0.3074	0.164
5	Benzene	2.27	1.5589	0.10	0.00	0.297	0.416	−0.0336	0.7163	−0.0148	−0.0336	0.3581	0.111
6	Toluene	2.38	1.4969	0.11	0.00	0.315	0.382	0.0291	0.6998	0.0132	0.0291	0.3499	0.099
7	o-Xylene	2.57	1.5054	0.16	0.00	0.343	0.387	0.0606	0.7423	0.0268	0.0606	0.3712	–
8	Diethylether	4.34	1.3497	0.47	0.00	0.526	0.291	0.3788	0.8551	0.1681	0.3788	0.4275	0.117
9	Chloroform	4.81	1.4459	0.10	0.20	0.559	0.352	0.3709	0.9753	0.1483	0.3709	0.4876	0.259
10	Ethyl acetate	6.02	1.3724	0.45	0.00	0.625	0.306	0.4891	0.9958	0.1996	0.4891	0.4979	0.228
11	*n*-Butyl acetate	6.17	1.3719	0.45	0.00	0.632	0.306	0.4977	1.0038	0.0202	0.4977	0.5019	0.241
12	THF	7.58	1.4072	0.55	0.00	0.686	0.328	0.5491	1.1023	0.2096	0.5491	0.5511	0.207
13	DCM	8.93	1.4242	0.10	0.13	0.725	0.339	0.5903	1.1660	0.2171	0.5902	0.5830	0.309
14	1-Octanol	9.80	1.4290	0.81	0.77	0.745	0.342	0.6138	1.1958	0.2222	0.6138	0.5979	0.537
15	1-Heptanol	11.30	1.4240	0.94	0.83	0.774	0.339	0.6518	1.2272	0.2331	0.6518	0.6136	0.549
16	1-Hexanol	13.00	1.4180	0.84	0.8	0.800	0.335	0.6861	1.2536	0.2432	0.6861	0.6268	0.559
17	1-Butanol	17.40	1.3990	0.84	0.84	0.845	0.323	0.7494	1.2917	0.2633	0.7494	0.6459	0.586
18	iso-Butanol	17.93	1.3959	0.84	0.79	0.849	0.321	0.7556	1.2938	0.2656	0.7556	0.6469	0.552
19	2-Propanol	19.92	1.3772	0.84	0.76	0.863	0.309	0.7787	1.2919	0.2762	0.7787	0.6459	0.546
20	Acetone	20.56	1.3587	0.48	0.08	0.867	0.297	0.7894	1.2777	0.2841	0.7894	0.6389	0.355
21	1-Propanol	20.60	1.3850	0.83	0.78	0.867	0.314	0.7812	1.3048	0.2746	0.7812	0.6524	0.617
22	Ethanol	24.55	1.3614	0.75	0.86	0.887	0.299	0.8129	1.3049	0.2887	0.8129	0.6525	0.654
23	Benzonitrile	26.00	1.5280	0.37	0.00	0.892	0.400	0.7650	1.4757	0.2363	0.7650	0.7379	0.333
24	Methanol	32.66	1.3284	0.66	0.98	0.913	0.276	0.8546	1.3021	0.3086	0.8546	0.6510	0.762
25	DMF	36.71	1.4305	0.69	0.00	0.922	0.343	0.8359	1.4196	0.2744	0.8356	0.7098	0.386
26	Acetonitrile	38.80	1.3442	0.40	0.19	0.926	0.287	0.8660	1.3348	0.3060	0.8660	0.6674	0.460
27	Ethylene glycol	41.40	1.4318	0.86	0.75	0.930	0.344	0.8457	1.4315	0.2762	0.8457	0.7157	0.790
28	DMSO	46.45	1.4793	0.76	0.00	0.938	0.372	0.8400	1.4880	0.2630	0.8400	0.7440	0.444

[a] Lippert–Mataga solvent function (Eq. (7)).
[b] Bakhshiev solvent function (Eq. (8)).
[c] Kawski–Chamma–Viallet solvent function (Eq. (9)).

seen from Fig. 6, B3LYP method produces relatively higher HLG values compared to that of LDA and GGA methods. However, as a result of EF application in the x-direction, HLGs of ip1, ip2 and ip3 decrease except for the HLG computed using B3LYP for ip1 and HLGs computed using LDA and GGA methods. External EF applied in y- and z-directions does not significantly affect the HLGs computed with all of the methods. HLGs of ip1 and ip2 show similar behavior under applied EF_{xyz} and decrease slightly. HLG value of ip3 calculated by B3LYP method decreases exponentially whereas HLG calculated using LDA and GGA methods increases with tendency of decreasing in its values. Discrepancy behavior of ip3 can be attributed to the nature of NO_2 group and Cl atom located at *meta* position. This observation is supported by the earlier published paper in which (*E*)-4-chloro-2-((2-(4-nitrophenyl)hydrazone)methyl)phenol molecule including *para*-NO_2 and *meta*-Cl shows similar behavior [63]. Consequently, ip1 and ip2 molecules have the tendency to behave as organic semiconductor under increasing external EF. ip3 tends to be in insulator form because HLG increases with the effect of EF.

The applied EFs induce charge transfer of the molecules and thus dipole moment of molecule changes linearly and exponentially. Fig. 7 shows electric dipole moment versus applied EFs in x-, y-, z-, and xyz-directions. EF applied in x-, y-, and z-directions gives rise to dipole moment change linearly.

Applied EF in xyz-direction leads to dipole moment calculated by LDA and GGA that increases exponentially while B3LYP computed dipole moment value increases with decreasing value exponentially. Dipole moment of ip2 calculated by LDA and GGA is exponentially expanded to higher value while the one calculated by B3LYP increases linearly as a result of EF in xyz-direction. Applied EF in three directions by LDA and GGA methods induces dipole moment of ip3 and gives rise to decrease exponentially whereas B3LYP computed dipole moment for

Table 4
Spectral treatment of the Lippert–Mataga, Bakhshiev, Kawski–Chamma–Viallet and Reichardt correlations of the studied compounds.

Equation	Slope (m)	Intercept	Correlation (R^2)	Solvents used in correlation	n
ip1					
Lippert–Mataga	$m_{L-M}=1747.5$	10,522	0.9107	4, 7, 8–10, 18, 20, 23, 26, 27	10
Bakhshiev	$m_B=577.87$	10,539	0.9188	4, 7–10, 13, 18, 20, 23, 26, 27	11
Kawski–Chamma–Viallet	$m_{K-C-V}=2929.8$	25,944	0.9590	22, 23, 26, 27	4
Reichardt	$m_R=7268$	5553.8	0.9592	17, 19, 22, 25, 27, 28	6
ip2					
Lippert–Mataga	$m_{L-M}=9618.2$	4669.9	0,9430	14–18, 21, 22, 24, 28	9
Bakhshiev	$m_B=386.81$	7603.8	0.9369	5, 7, 9, 10, 13, 26, 27	7
Kawski–Chamma–Viallet	$m_{K-C-V}=1224.7$	22,915	0.9078	1–3, 5, 7, 10, 12, 16–19, 21–23, 28	15
Reichardt	$m_R=3561.6$	5071.1	0.9197	14–19, 21, 22, 24, 27	10
ip3					
Lippert–Mataga	$m_{L-M}=8531.8$	8239.8	0.9277	6, 8, 15, 16, 19, 21, 27	7
Bakhshiev	$m_B=2910$	8136.7	0.9839	6, 15, 16, 19, 21, 27	6
Kawski–Chamma–Viallet	$m_{K-C-V}=7383.5$	28,180	0.9447	12, 16, 19, 21, 27	5
Reichardt	$m_R=4154.7$	7728.3	0.9527	6, 12, 15, 16, 19, 21, 27	7

Table 5
Onsager cavity radius, ground state and excited state dipole moments (in Debye).

	Onsager radius '*a*' (Å)	μ_g[a]	$\mu_{e(L-M)}$[b]	$\mu_{e(B)}$[c]	$\mu_{e(K-C-V)}$[d]	$\mu_{e(R)}$[e]	(μ_e/μ_g)[f]
ip1	4.221	4.236	7.856	6.345	6.318	8.289	1.491
ip2	4.099	1.782	9.987	3.427	3.428	4.497	1.926
ip3	4.327	3.709	11.971	8.534	8.534	6.889	2.301

$1D = 3.33564 \times 10^{-30}$, C. m. $= 10^{-18}$ esu·cm.
[a] Calculated according to Eq. (10).
[b] Calculated according to L–M correlation, Eq. (4).
[c] Calculated according to B correlation, Eq. (5).
[d] Calculated according to K–C–V correlation, Eq. (6).
[e] Calculated according to R correlation Eq. (14).
[f] Calculated according to Eq. (12).

ip3 increases linearly. For the zero field, dipole moments are calculated as 1.8022 D, 1.7564 D, and 2.3842 D for ip1, 4.7853 D, 4.3032 D, and 4.1716 D for ip2 and 4.2490 D, 4.2321 D, and 4.2473 D for ip3 in xyz-direction by LDA, GGA and B3LYP methods, respectively. As the field increases to 0.20 V/Å, dipole moment of ip1 increases to 2.4458 D, 3.9482 D, and 3.5677 D, and dipole moment of ip2 increases to 8.2145 D, 7.6035 D, and 4.6707 D with the applied EF in xyz-direction by LDA, GGA and B3LYP methods, respectively. Dipole moment calculated by LDA and GGA methods of ip3 reduces to 2.5971 D, 2.6074 D and B3LYP calculated dipole moment increases to 5.5939 D, respectively. Discrepancy between experimental and theoretical dipole moment attributed to that theoretical value is obtained in vacuum while experimental value is determined in solid state.

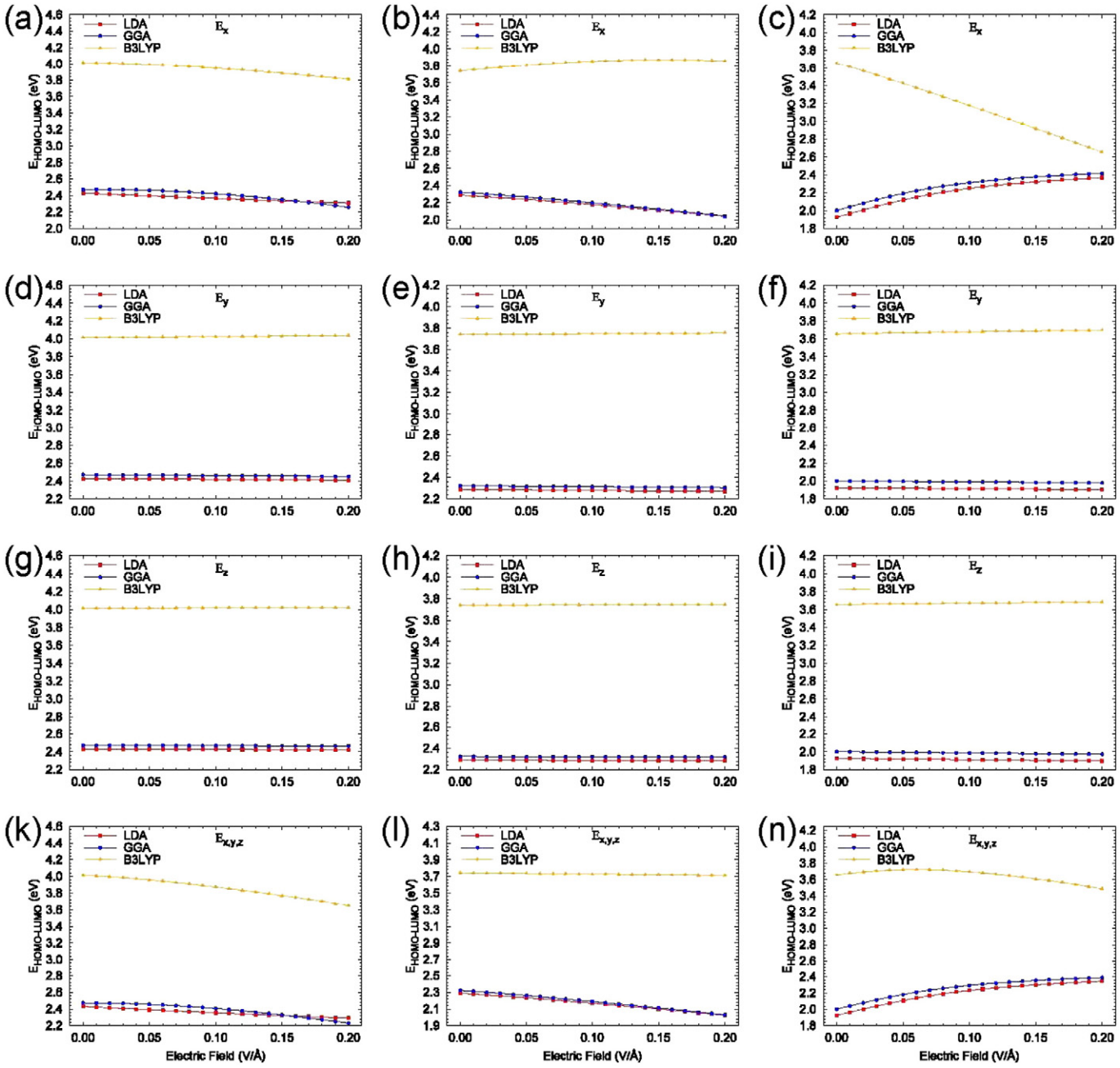

Fig. 6. HOMO–LUMO gap (HLG) as a function of the external electric field calculated by GGA, LDA and B3LYP/6-31G(d,p) methods for ip1 ((a), (d), (g), (k)), ip2 ((b), (e), (h), (l)) and ip3 ((c), (f), (i), (n)).

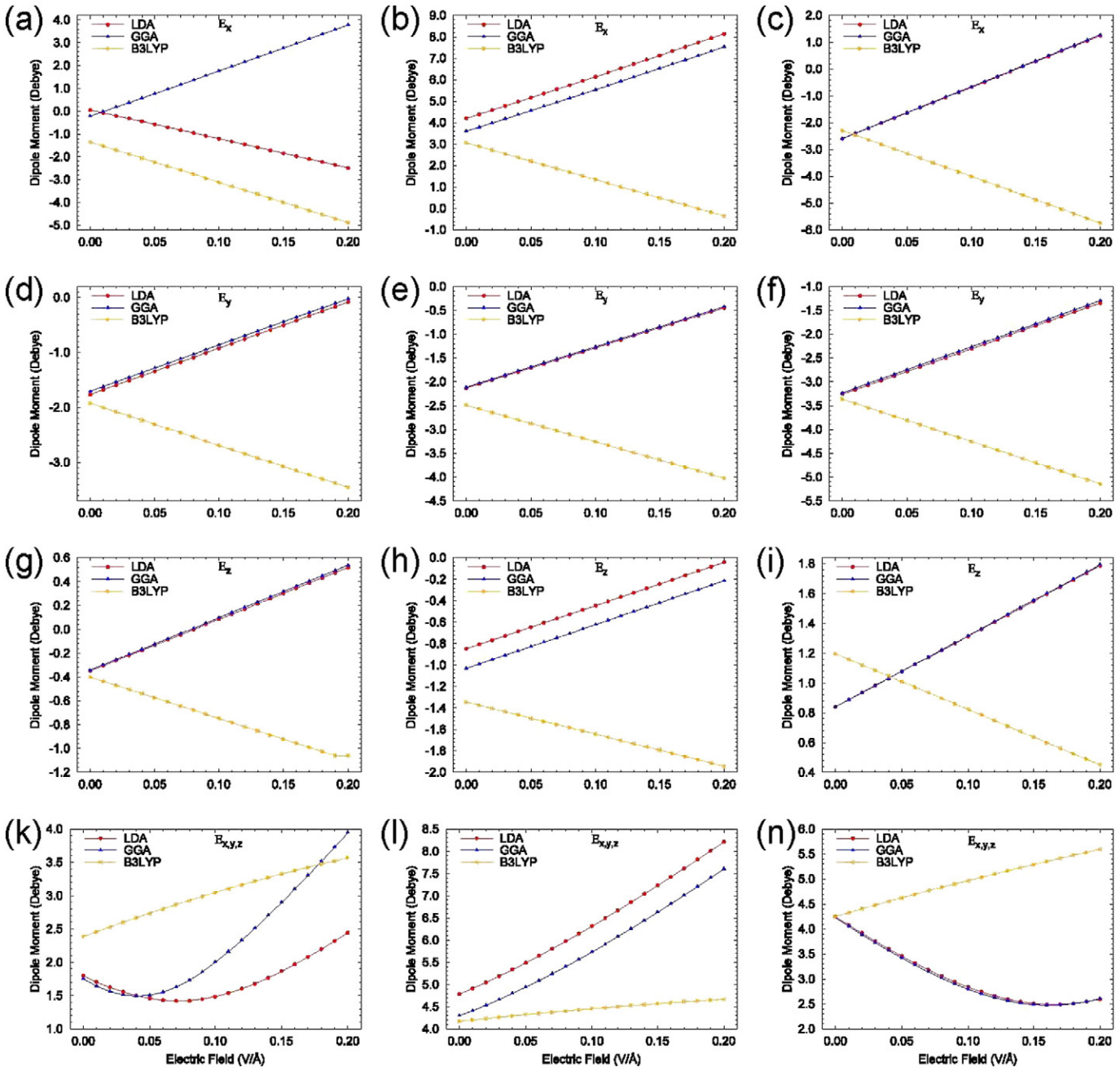

Fig. 7. Dipole moment as a function of the external electric field calculated by GGA, LDA and B3LYP/6-31G(d,p) methods for ip1 ((a), (d), (g), (k)), ip2 ((b), (e), (h), (l)) and ip3 ((c), (f), (i), (n)).

3.4. Density of states (DOS)

Density of states versus energy plots for EF = 0 V/Å and EF = 0.20 V/Å and HOMO, LUMO plots calculated by GGA method are shown in Figs. 8 and 9 (The DOS and HOMO, LUMO plots obtained by LDA and B3LYP methods present similar results and could not be given here.). Dotted lines in DOS plots indicate Fermi Level (E_F). As can be seen from Fig. 8, the HOMO and LUMO are predominantly localized on phenol system and CH = N for ip1 in the absence of EF. However, the magnitude of LUMO localized on CH = N is observed as larger than that of HOMO. Applying EF in xyz-direction gives rise to HOMO that localizes over entire molecule while LUMO nearly stays stable.

HOMO plot of ip2 shows that orbitals are localized on aniline moiety, CH = N bridge and OH group while LUMO seems to migrate to CH = N bridge in the lack of EF. Applied 0.20 V/Å EF in xyz-direction leads the HOMO to migrate towards aniline but it does not induce LUMO significantly.

HOMO orbitals of ip3 are mainly localized on chlorophenol and LUMO plot shows that orbitals migrate to nitrophenyl moiety in the state of EF = 0 V/Å. 0.20 V/Å electric field does not change the HOMO orbital location, but LUMO orbitals migrate to chlorophenol and CH = N moieties.

DOS plots also indicate the HOMO, LUMO energy levels of ip1, ip2 and ip3 molecules.

3.5. Solvatochromic treatments of the investigated Schiff base molecules

The solvent-induced spectral shifts of electronic transitions can be described with the effect of solvent parameters. These spectral shifts

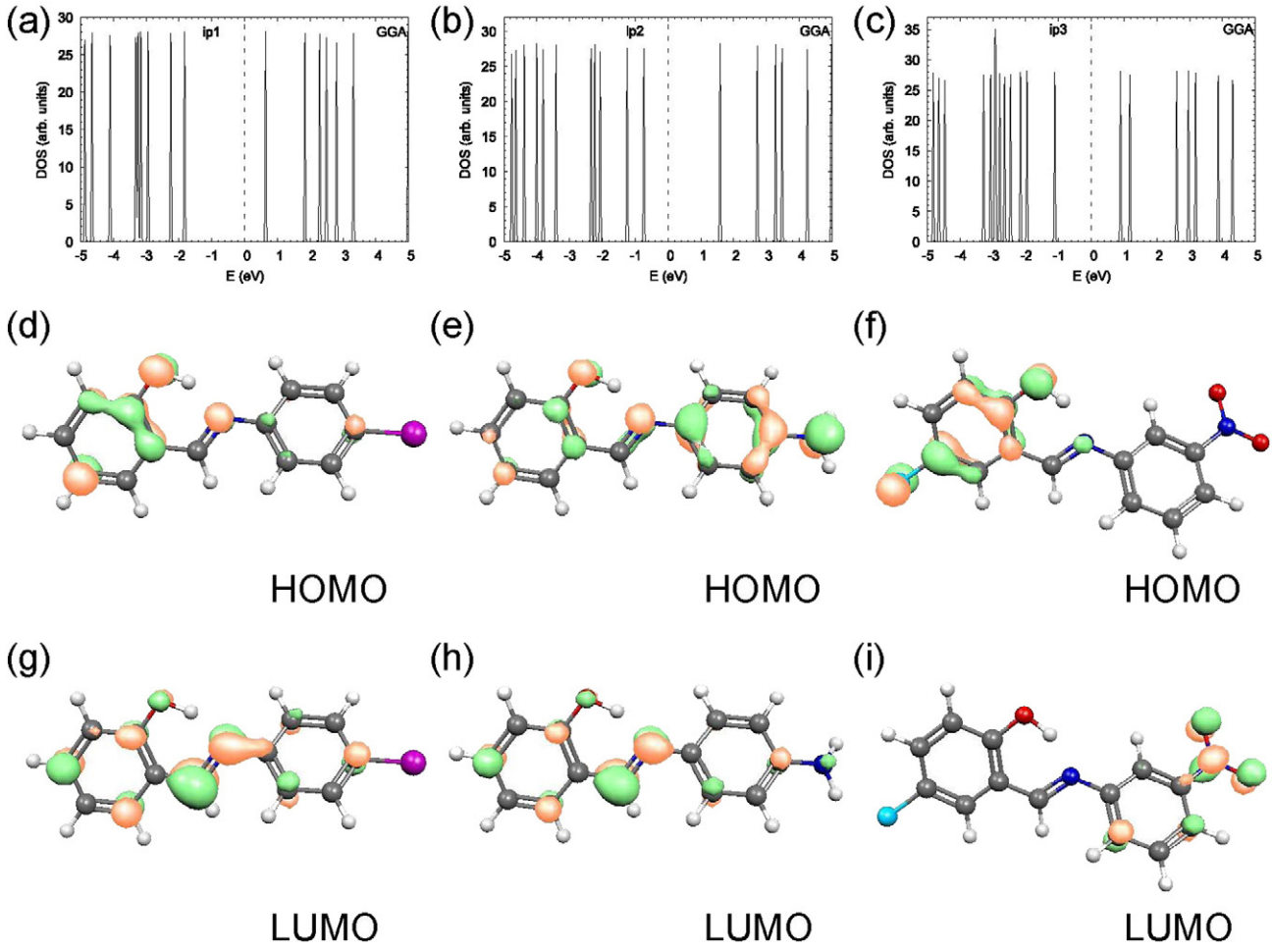

Fig. 8. Density of states (DOS) versus energy and HOMO, LUMO plots calculated by GGA in E = 0 V/Å state for ip1 ((a), (d), (g)), ip2 ((b), (e), (h)) and ip3 ((c), (f), (i)).

have been researched using LSERs. The LSER method is carried out using the solvent parameters as independent variables and wavelengths of absorption and emission spectra as dependent variables. The LSER coefficients, number of used solvent using LSER calculations, and statistical parameters from both maximum absorption band and maximum emission band of investigated molecules are listed in Tables 6 and 7, respectively. Statistical parameters, R^2, R, F and P, are derived from multiple linear regression analysis.

R is the linear correlation coefficient, which measures the strength and the direction of a linear relationship between dependent and independent variables. R^2 determines the linear correlation coefficient, which gives the proportion of the fluctuation of variables. $R \geq 0.7$, $R^2 \geq 0.7$, bigger F values and zero about P values have affected viability of LSER results. Thus, the values of statistical parameters give an occasion to limited number of used solvents.

The solvatochromic behaviors of investigated molecules have been researched in different three group solvents. The first groups are nonpolar solvents such as n-pentane, n-hexane, cyclohexane, benzene, toluene and chloroform. The second groups are polar protic solvents such as methanol, ethanol, 1-propanol, 2-propanol, iso-butanol, 1-butanol, 1-hexanol, 1-heptanol and 1-octanol. The last groups are polar aprotic solvents such as benzonitrile, DMSO, acetone, 1,4-dioxane, etylene glycol, acetonitrile, DMF, o-xylene, DCM (dichloromethane), THF, n-ethyl acetate and n-butyl acetate.

The sign and magnitude of coefficients derived from LSERs indicate the degree of different solute–solvent interactions. The LSER calculations for maximum electronic absorption transition of ip1 and ip2 molecules have been carried out by using 28 solvents, while LSER calculation for maximum electronic absorption transition of ip3 molecule is performed by using 25 solvents. According to Table 6, the C_1 coefficient is negative, while the C_2 coefficient is positive. $|C_1|$ value has bigger than $|C_2|$. The C_1 coefficient measures the dispersion interaction effect (refractive index function) in electronic absorption spectra, while the C_2 coefficient measures the effect of dipolar interaction (dielectric function). So, we can say from Table 6 that electronic transitions of all the investigated molecules exhibit bathochromic effect (red shift) dependent on dispersion–polarization forces. In that, existed electronic transitions in all molecules have been affected by dispersion–polarization interaction more than that of dipolar induction interactions. For ip1 and ip2 molecules, $|C_3|$ value is bigger than $|C_4|$ value. Thus, π–π* electronic transitions of aforesaid two molecules have occurred by the larger effect of H-bond accepting ability in accordance with H-bond donor ability. But, π–π* electronic transition of ip3 molecule occurs to H-bond donor ability of solvents due to $|C_4| > |C_3|$. The dipole moments of ip1 and ip3 molecule increase in excitation state with more controlled orientation–induction interactions and dispersion–polarization interactions, which are non-specific (global) interactions. In contrast, the dipole moment of the ip2 molecule increases excitation state with effect on orientation–induction interaction and H-bond acceptor ability. The high absolute values of coefficient C_3 compared to C_4 cause a red shift (bathochromic effect) in electronic absorption spectra of ip1 and ip2 molecules, while the small absolute values of coefficient C_3 compared to C_4 cause a blue shift (hypsochromic effect) in electronic absorption spectra of ip3 molecule. These bathochromic effects correspond to more stabilized excited state as compared to ground state.

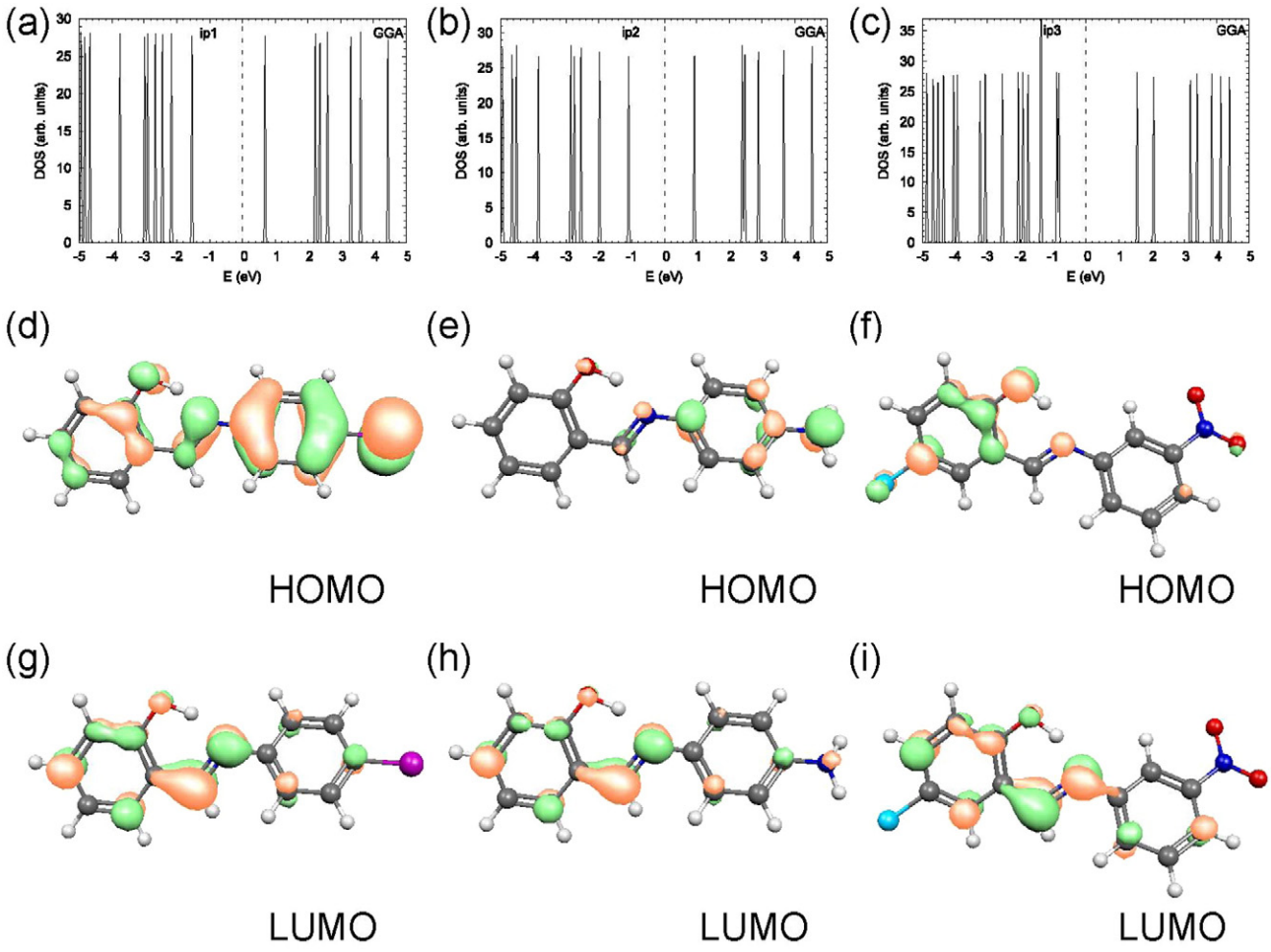

Fig. 9. Density of states (DOS) versus energy and HOMO, LUMO plots calculated by GGA in $E_{xyz} = 0.20$ V/Å state for ip1 ((a), (d), (g)), ip2 ((b), (e), (h)) and ip3 ((c), (f), (i)).

The LSER calculations for maximum electronic emission transition of ip1, ip2 and ip3 molecules have been done by using a number of 17, 10 and 18 solvents, respectively. R^2 and R values given in Table 7 indicate acceptability of statistical parameters of ip1 and ip3 molecules. However, obtained statistical parameters from LSER calculations have not been given satisfactory results for ip2 molecule. The fundamental reason of this state is that electronic emission transitions of investigated molecules have occurred by the steric, mezomeric and inductive effects. Nonetheless, LSER calculations do not consider these effects directly.

We can say from the results given in Table 7 that absolute C_1 values derived from LSER of ip1 and ip2 molecules are bigger than absolute C_2 values derived from LSER. Thus, investigated electronic emission transitions are found as more effective on dispersion polarization interactions in comparison to orientation–induction interactions. However, this interpretation has not been obtained for ip2 molecule. According to |C1| and |C2| values, we can say that fluorescence band maxima of the investigated molecule indicate bathochromic shift. It is observed that absolute C_3 value is bigger than absolute C_4 value of ip1 and ip3 molecules, when absolute C_3 value is smaller than absolute C_4 value of ip2 molecule. This indicates that the H-bond acceptor ability effect is weaker than the H-bonding donor ability in electronic emission transitions of ip1 and ip3 molecules, when H-bond donor ability effects are weaker than the H-bonding acceptor ability in electronic emission transitions of ip2 molecule. The high absolute value of C_3 compared to C_4 reveals a tendency towards bathochromic effect of electronic emission spectra, while in inverse state, the small absolute value of C_3 compared to C_4 reveals a tendency towards hypsochromic effect of electronic emission spectra. Thus, we have observed that electronic emission spectra of ip2 and ip3 molecules have done red shifts depending on dielectric coefficients of using solvents, while electronic emission spectra of ip1 molecule exhibit blue shifts depending on dielectric constant of solvents. In Table 7, electronic emission transition of ip3 molecule is mostly controlled by H-bond acceptor ability of solvents.

4. Conclusions

In this study, the ground and excited state dipole moments of some Schiff base derivatives have been determined by using solvatochromic shift methods. The excited state dipole moments are found larger than ground state dipole moment which reveals that molecules are more

Table 6
LSER coefficients and statistical parameters from the maximum absorption band of investigated molecules.

Molecules	C_0 (cm^{-1})	C_1	C_2	C_3	C_4	R^2	R	F	P	Number of solvent
ip1	29,343.65	−1319.80	565.60	−234.56	67.47	0.694	0.833	13.068	0.000	28
ip2	28,102.46	−4505.57	50.62	−1225.33	25.92	0.960	0.980	137.814	0.000	28
ip3	28,271.46	−1099.87	806.14	127.69	−271.03	0.695	0.834	11.380	0.000	25

Table 7
LSER coefficients and statistical parameters from the maximum emission band of investigated molecules.

Molecules	C_0 (cm^{-1})	C_1	C_2	C_3	C_4	R^2	R	F	P	Number of solvent
ip1[a]	18,025.27	339.41	235.33	−123.20	294.75	0.684	0.827	6.497	0.005	17
ip2[b]	18,464.95	−62.65	35.30	−28.04	−6.39	0.452	0.672	1.029	0.474	10
ip3[c]	14,182.10	7898.63	6124.60	−3071.27	36.83	0.674	0.821	6.732	0.004	18

[a] LSER calculations have not joined to maximum emission band in n-pentane, 1.4-dioxane, diethylether, THF, DCM, 1-butanol, 2-propanol, ethanol, methanol, DMF and DMSO solvents.
[b] LSER calculations have been derived by using n-hexane, cyclohexane, 1.4-dioxane, toluene, 1-butanol, acetonitril, acetone, ethanol, methanol and DMSO.
[c] LSER calculations have not joined to maximum emission band in benzene, 2-propanol, 1-propanol and ethylene glycol.

polar in the excited state than those in the ground state. Increasing electric field in xyz-direction appreciably gives rise to dipole moment change exponentially. However, the increase of electric field leads to HOMO–LUMO gap of ip3 that tends to increase. Considering the HOMO–LUMO gap and dipole moment changes under applied external electric field, ip1 and ip2 molecules have a tendency to behave as organic semiconductor under increasing external EF. ip3 tends to be in insulator form because HLG increases with the effect of EF. These observations give an insight on the Schiff base molecules that they can be designable as insulator or conductor which makes them candidates for use in design of electronic devices and organic photovoltaic cells.

Acknowledgment

The authors greatly acknowledge the support of Bitlis Eren University, Scientific and Technological Application and Research Center.

The authors greatly appreciate Bitlis Eren University Research Foundation for financial support. Project number: BEBAP-2014.05.

Appendix A. Supplementary data

Supplementary data to this article can be found online at http://dx.doi.org/10.1016/j.molliq.2015.01.056.

References

[1] Z. Liang, Z. Liu, L. Jiang, Y. Gao, Tetrahedron Lett. 48 (2007) 1629.
[2] Y. Liu, H. Wang, L.-H. Wang, Z. Li, H.-Y. Zhang, Q. Zhang, Tetrahedron 59 (2003) 7967.
[3] Z. Liang, Z. Liu, Y. Gao, Tetrahedron Lett. 48 (2007) 3587.
[4] A. Chattopadhyay, M. Meier, S. Ivaninskii, P. Burkhard, Biochemistry 46 (2007) 8315.
[5] N.P. Bazhulina, Y.V. Morozov, A.I. Papisova, T.V. Demidkina, Eur. J. Biochem. 267 (2000) 1830.
[6] A. Tramonti, R.A. John, F. Bossa, D. de Biase, Eur. J. Biochem. 269 (2002) 4913.
[7] B. Campanini, F. Schiaretti, S. Abbruzzetti, D. Kessler, A. Mozzarelli, J. Biol. Chem. 281 (2006) 38769.
[8] J.M. Lehn, Supramolecular Chemistry, Wiley-VCH, Wenham, 1995.
[9] E. Ispir, Dyes Pigments 82 (2009) 13–19.
[10] K. Ogawa, J. Harada, J. Mol. Struct. 647 (2003) 211–216.
[11] T.S. Basu Baul, P. Das, A.K. Chandra, S. Mitra, Dyes Pigments 82 (2009) 379–386.
[12] H. Khanmohammadi, A. Abdollahi, Dyes Pigments 94 (2012) 163–168.
[13] A.A. Alemi, B. Shaabani, Acta Chim. Slov. 47 (2000) 363–369.
[14] C.C. Ersanli, C. Albayrak, M. Odabas_oglu, C. Thone, A. Erdonmez, Acta Crystallogr. E60 (2004) o133–o0135.
[15] B. Koşar, C. Albayrak, M. Odabasoglu, O. Buyukgüngor, Acta Crystallogr. E61 (2005) o2106–o02108.
[16] H. Nazir, M. Yildiz, H. Yilmaz, M.N. Tahir, D. Ulku, J. Mol. Struct. 524 (2000) 241–250.
[17] P. Gilli, V. Bertolasi, L. Pretto, A. Lycka, G. Gilli, J. Am. Chem. Soc. 124 (2002) 13554–13567.
[18] P. Simunek, V. Bertolasi, V. Machacek, J. Mol. Struct. 642 (2002) 41–51.
[19] P. Gilli, V. Bertolasi, L. Pretto, G. Gilli, J. Mol. Struct. 790 (2006) 40–49.
[20] O.A. Adegoke, M. Ghosh, A. Jana, J. Mol. Liq. 174 (2012) 17–25.
[21] E. Hadjoudis, I.M. Mavridis, Chem. Soc. Rev. 33 (2004) 579.
[22] E.D. Raczynska, W. Kosinska, B. Osmiałowski, R. Gawinecki, Chem. Rev. 105 (2005) 3561.
[23] G.-Y. Yeap, S.-T. Ha, N. Ishizawa, K. Suda, P.-L. Boey, W.A.K. Mahmood, J. Mol. Struct. 658 (2003) 87.
[24] P. Przybylski, M. Włodarz, G. Schroeder, R. Pankiewicz, B. Brzezinski, F. Bartl, J. Mol. Struct. 693 (2004) 95.
[25] H. Dal, Y. Suzen, E. Sahin, Spectrochim. Acta A 67 (2007) 808.
[26] O.N. Kadkin, H. Han, Y.G. Galyametdinov, J. Organomet. Chem. 692 (2007) 5571.
[27] J. Costamagna, L.E. Lillo, B. Matsuhiro, M.D. Noseda, M. Villagran, Carbohydr. Res. 338 (2003) 1535.
[28] Y. Gülseven Sıdır, İ. Sıdır, H. Berber, G. Türkoğlu, J. Mol. Liq. 199 (2014) 57–66.
[29] A.L. Iglesias, G. Aguirre, R. Somanathan, M. Parra-Hake, Acta Crystallogr. E62 (2006) o390.
[30] T. Akitsu, Y. Einaga, Acta Crystallogr. E62 (2006) o4315.
[31] M. Ghasemian, A. Kakanejadifard, F. Azarbani, A. Zabardasti, S. Kakanejadifard, J. Mol. Liq. 195 (2014) 35–39.
[32] H. Dürr, H. Bouas-Laurent, Photochromism: Molecules and Systems, Elsevier, Amsterdam, 1990. 685–710.
[33] A.D. Garnovskii, A.L. Ninorozhkin, V.I. Minkin, Coord. Chem. Rev. 126 (1993) 1.
[34] R. Lozier, R.A. Bogomolni, W. Stoekenius, Biophys. J. 15 (1975) 955–962.
[35] E. Hadjoudis, M. Vitterakis, I. Moustakali-Mavridis, Tetrahedron 43 (1987) 1345–1360.
[36] F. Milia, E. Hadjoudis, J. Seliger, J. Mol. Struct. 177 (1988) 191–197.
[37] G. Pistolis, D. Gegiou, E. Hadjoudis, J. Photochem. Photobiol. A Chem. 93 (1996) 179–184.
[38] K. Amimoto, T. Kawato, J. Photochem. Photobiol. C 6 (2005) 207.
[39] C.O. Sánchez, J.C. Bernede, I. Cattin, M. Makha, N. Gatica, Thin Solid Films 562 (2014) 495–500.
[40] J. Tomczak, K. Dobek, J. Lumin. 129 (2009) 884–891.
[41] L. Bilot, A. Kawski, Z. Naturforsch. 17a (1962) 621–627.
[42] A. Kawski, in: J.F. Rabek (Ed.), Progress in Photochemistry and Photophysics, vol. 5, CRC Press, Boca Raton, USA, 1992, pp. 1–47.
[43] E. Lippert, Z. Naturforsch. 10a (1955) 541–545.
[44] A. Chamma, P. Viallet, C. R. Acad. Sci. Paris C 270 (1970) 1901–1904.
[45] M. Ravi, T. Soujanya, A. Samantha, T.P. Radhakrishnan, J. Chem, Soc. Faraday Trans. 91 (1995) 2739–2742.
[46] Y. Fenar, Anilin ve Hidrazin Türevi Schiff Bazlarının Sentezi, Yapılarının Aydınlatılması ve Farklı Çözücülerde Solvatokromik Özelliklerinin UV–vis ve Floresans Spektroskopisi ile Tayini, Lisans Tezi Anadolu Üniversitesi, Fen Fakültesi, Kimya Bölümü, Eskişehir, 2011.
[47] C. Reichardt, Solvents and Solvent Effects in Organic Chemistry, VCH, New York, 2005.
[48] D.R. Lide (Ed.), Handbook Chemistry and Physics, 76th ed.CRC Press, Boca Raton, Florida, 1995.
[49] D.R. Lide (Ed.), 80th ed., CRC Press, New York, 1999.
[50] C. Reichardt, in: H. Ratajczak, W.J. Orville-Thomas (Eds.), Molecular Interactions, vol. 3, John Wiley & Sons Ltd., 1982
[51] A.D. Becke, J. Chem. Phys. 98 (1993) 5648–5653.
[52] M.J. Frisch, G.W. Trucks, H.B. Schlegel, G.E. Scuseria, M.A. Robb, J.R. Cheeseman, G. Scalmani, V. Barone, B. Mennucci, G.A. Petersson, H. Nakatsuji, M. Caricato, X. Li, H. P. Hratchian, A.F. Izmaylov, J. Bloino, G. Zheng, J.L. Sonnenberg, M. Hada, M. Ehara, K. Toyota, R. Fukuda, J. Hasegawa, M. Ishida, T. Nakajima, Y. Honda, O. Kitao, H. Nakai, T. Vreven, J.A. Montgomery Jr., J.E. Peralta, F. Ogliaro, M. Bearpark, J.J. Heyd, E. Brothers, K.N. Kudin, V.N. Staroverov, R. Kobayashi, J. Normand, K. Raghavachari, A. Rendell, J.C. Burant, S.S. Iyengar, J. Tomasi, M. Cossi, N. Rega, J.M. Millam, M. Klene, J.E. Knox, J.B. Cross, V. Bakken, C. Adamo, J. Jaramillo, R. Gomperts, R.E. Stratmann, O. Yazyev, A.J. Austin, R. Cammi, C. Pomelli, J.W. Ochterski, R.L. Martin, K. Morokuma, V.G. Zakrzewski, G.A. Voth, P. Salvador, J.J. Dannenberg, S. Dapprich, A.D. Daniels, Farkas, J.B. Foresman, J.V. Ortiz, J. Cioslowski, D.J. Fox, Gaussian 09, Revision A.1, Gaussian, Inc., Wallingford CT, 2009.
[53] J.M. Soler, E. Artacho, J.D. Gale, A. García, J. Junquera, P. Ordejón, D. Sánchez-Portal, J. Phys. Condens. Matter 14 (2002) 2745.
[54] J.P. Perdew, K. Burke, M. Ernzerhof, Phys. Rev. Lett. 77 (1996) 3865–3868.
[55] J.P. Perdew, A. Zunger, Phys. Rev. B 23 (1981) 5048–5079.
[56] N. Troullier, J.L. Martins, Phys. Rev. B 43 (1991) 1993–2006.
[57] L. Kleinman, D.M. Bylander, Phys. Rev. Lett. 48 (1982) 1425–1428.
[58] P. Suppan, Chem. Phys. Lett. 3 (1983) 272–275.
[59] Bernard Valeur, Molecular florescence, Principles and Applications, Wiley, Federal Republic of Germany, 2002.
[60] İsmet Kaya, Sermet Koyuncu, Iran. Polym. J. 16 (4) (2007) 261–270.
[61] Corwin Hansch, A. Leo, R.W. Taft, Chem. Rev. 91 (2) (1991) 165–195.
[62] Paula Yurkanis Bruice, Organic Chemistry, Fourth edition, May 1 2003. 643–668 (Hardcover, by (Author)).
[63] İ. Sıdır, Y. Gülseven Sıdır, F. Demiray, H. Berber, J. Mol. Liq. 197 (2014) 386–394.